Enhanced Red Emissions of Europium (III) Chelates in RNA–OTMA Complexes

Lijuan Liang [1], Nianjie Zhang [1], Rong Cao [1], Suyun Wang [1], Shengzhen Liu [1], Zhaohui Yu [1], Quanxiao Liu [1], Jigang Wang [1,*], Zhenjun Li [2,*] and Tao Jiang [3,*]

[1] Beijing Key Laboratory of Printing and Packaging Materials and Technology, Beijing Institute of Graphic Communication, Beijing 102600, China
[2] GBA Research Innovation Institute for Nanotechnology, Guangzhou 510700, China
[3] CAS Center for Excellence in Nanoscience, Beijing Key Laboratory of Micro-Nano Energy and Sensor, Beijing Institute of Nanoenergy and Nanosystems, Chinese Academy of Sciences, Beijing 101400, China
* Correspondence: jigangwang@bigc.edu.cn (J.W.); lizhenjun@nanoctr.cn (Z.L.); jiangtao@binn.cas.cn (T.J.)

Abstract: In recent years, biopolymers have been widely used in optoelectronic devices because of their unique structure, novel optical and physical properties. In this paper, novel RNA-based photofunctional materials were fabricated by associating an RNA–OTMA (octadecyltrimethylammonium chloride) lipid complex with a luminescent Eu (III) complex. The fluorescence emission intensity, fluorescence quantum yield and fluorescence lifetime were characterized in both solution and thin film states, and the interaction between the RNA–OTMA lipid complex and Eu (III) complexes was analyzed. This study suggests that the luminescence performance of the Eu (III) complexes doped with RNA–OTMARNA–OTMA was significantly enhanced compared with those of the complex in a conventional poly (methyl methacrylate) matrix, thereby providing an important basis for the application of biomaterials in optoelectronic devices.

Keywords: RNA–OTMA; Eu $(TTA)_3$ $(H_2O)_2$; emission intensity; fluorescence quantum yield

1. Introduction

In recent years, biopolymers have attracted extensive research interest due to the advantages of excellent biodegradability, biocompatibility and a wide range of chemical applications [1,2]. Deoxyribonucleic acid (DNA), for instance, has a unique double helix structure, that allows it to incorporate a variety of functional materials with good properties, such as electrostatic, intercalation and grooving [3]. Similar polymers include ribonucleic acid (RNA), a nucleic acid that also contains hydroxyl sequences of genetic instructions. The difference between RNA and DNA is that RNA usually contains only a single strand, but due to the existence of multiple free strands on the RNA backbone, the rotating-covalent bond combines the two steric isomers that exist in the sugar ring [4]. Therefore, the RNA backbone has a high degree of variability, and can also exhibit good properties similar to DNA. Due to the good material compatibility and easy processing, these polymers can be combined with highly conductive materials or chemically modified with other materials to make composites with multiple properties for applications in biomedicine [5], electronic devices [6], etc.

Biopolymer-based optoelectronic devices have attracted extensive attention in the preparation of various flexible circuits, sensors, and memory devices because of their flexible printable, foldable, and large-area preparation properties [7–10]. Hagen et al. [11] improved electroluminescence efficiency using DNA complexes as electron blocking layers in green and blue organic light-emitting diodes (OLEDs). Compared with similar OLEDs, the bio-OLED based on DNA material has 10 times higher luminous efficiency and 30 times higher brightness. Liang et al. [12] constructed a bio-thin film transistor (TFT)-based non-volatile memory (NVM) device using an RNA-CTMA complex as a dielectric layer,

which exhibited excellent memory characteristics and provided a new idea for preparing low-cost, environmentally friendly memories. In addition, luminescent lanthanide (III) complexes have been widely used in the fields of luminescent materials [13], biological detection [14], displays [15–17] and sensors [18–20] due to their narrow emission bands, stable performance and long emission lifetimes. In previous study, Ru $(bpy)_3^{2+}$ based red light-emitting diodes with fast start response were prepared by doping Ru $(bpy)_3^{2+}$ fluorescent materials into DNA [21]. In addition, the effect of DNA-CTMA on the luminescence properties of Eu (III) complexes was investigated by doping the Eu (III) complexes into DNA–CTMA [22]. The special structure of DNA can be used to effectively enhance the luminescence intensity of fluorescent substances, which has the potential to be applied in luminescent devices [23]. However, much research remains to be conducted on the interaction of RNA–OTMA complexes and Ln (III) complexes, as well as the effect of RNA–OTMA complexes on the luminescence properties of Ln (III) complexes.

In this work, we prepared luminescent red complex films containing RNA–OTMA and tris (2-thienyltrifluoroacetone) europium (III) [Eu $(TTA)_3$ $(H_2O)_2$] for the first time by doping luminescent lanthanide (III) complex with a RNA–OTMA lipid complex. The interactions of RNA–OTMA and the Eu (III) complex are discussed using absorption and circular dichroism spectra. The fluorescence emission spectra, fluorescence emission lifetimes and fluorescence quantum yields of RNA–OTMA/Eu $(TTA)_3$ $(H_2O)_2$ films with different doping ratios were also investigated. In comparison, we created PMMA/Eu $(TTA)_3$ $(H_2O)_2$ films using poly (methyl metha-crylate) (PMMA), a well-known conventional polymer. In this way, the mechanism of luminescence enhancement of rare earth europium complexes by RNA complexes was investigated in depth.

2. Experimental Section

2.1. Materials

RNA (from torula yeast, specification 25 g), octadecyltrimethylammonium chloride (OTMA), thienyl trifluoroacetone (TTA), europium acetate (Eu (III)) hydrate and polymethyl methacrylate (PMMA) were purchased from Sigma Aldrich (Shanghai, China) Trading Company, and the molecular structures of each substance are shown in Figure 1. The n-butanol and toluene were purchased from Xilong Chemical Co., Ltd., Shantou, China.

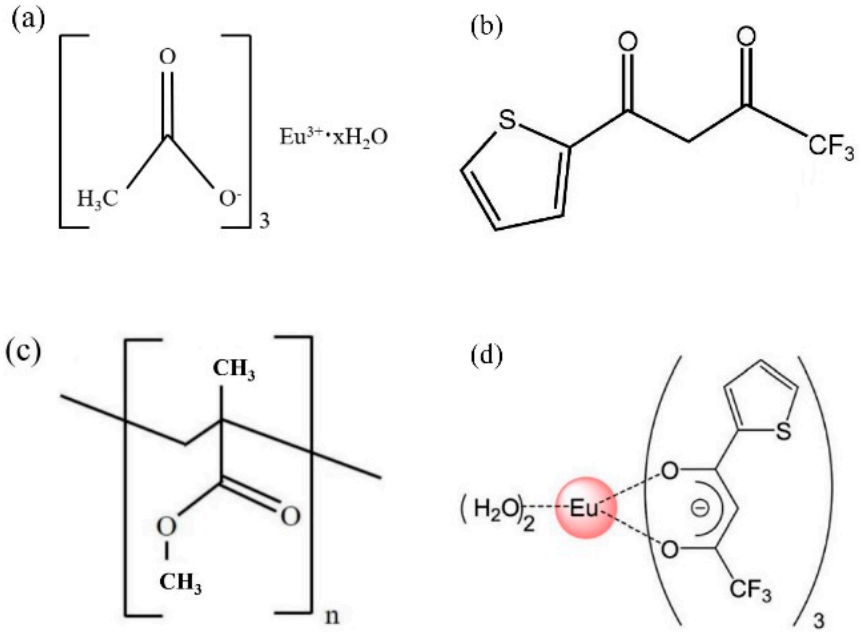

Figure 1. Schematic diagram of the structure of the experimental material: (**a**) europium acetate hydrate; (**b**) thiophenecarbonyl trifluoroacetone (TTA); (**c**)polymethyl methacrylate (PMMA); (**d**) tris (2-thienyl trifluoroacetone) europium (III) [Eu $(TTA)_3$ $(H_2O)_2$].

2.2. Preparation of Eu $(TTA)_3$ $(H_2O)_2$ Complexes

First, 3.34 g of thiopheneformyl trifluoroacetone (TTA), anhydrous ethanol and ammonia were mixed and dissolved, and left to stand for complete dissolution to prepare a TTA solution; next, 1.65 g of Eu (III) hydrate was completely dissolved to prepare. Then, the TTA solution and the Eu (III) aqueous solution were mixed, stirred, filtered and dried to obtain a precipitate; finally, the precipitate and mineral spirits were stirred at a certain temperature, filtered and dried to obtain the Eu $(TTA)_3$ $(H_2O)_2$ complex. The Eu $(TTA)_3$ $(H_2O)_2$ Eu $(TTA)_3$ $(H_2O)_2$ powder was dissolved in butanol solution, and the Eu $(TTA)_3$ $(H_2O)_2$ complex solution of different concentrations were prepared by stirring and dissolving.

2.3. Preparation of RNA–OTMA Lipid Complexes

RNA–OTMA lipid complexes were prepared using RNA and OTMA through an ion exchange reaction. RNA solution was made by mixing 0.201 g of RNA with 100 mL of deionized water, and OTMA solution was made by mixing 0.348 g of octadecyltrimethylammonium chloride (OTMA) with 100 mL of deionized water. The RNA complex with OTMA (RNA–OTMA) was prepared by the addition of aqueous solution of RNA to the OTMA solution. The solution was stratified with white flocculent precipitate appearing in the lower layer and the upper layer of the solution being transparent by stirring. With ultrapure water, the precipitate was filtered through thoroughly washed, then, we dried it under vacuum. The preparation process is shown in Figure 2.

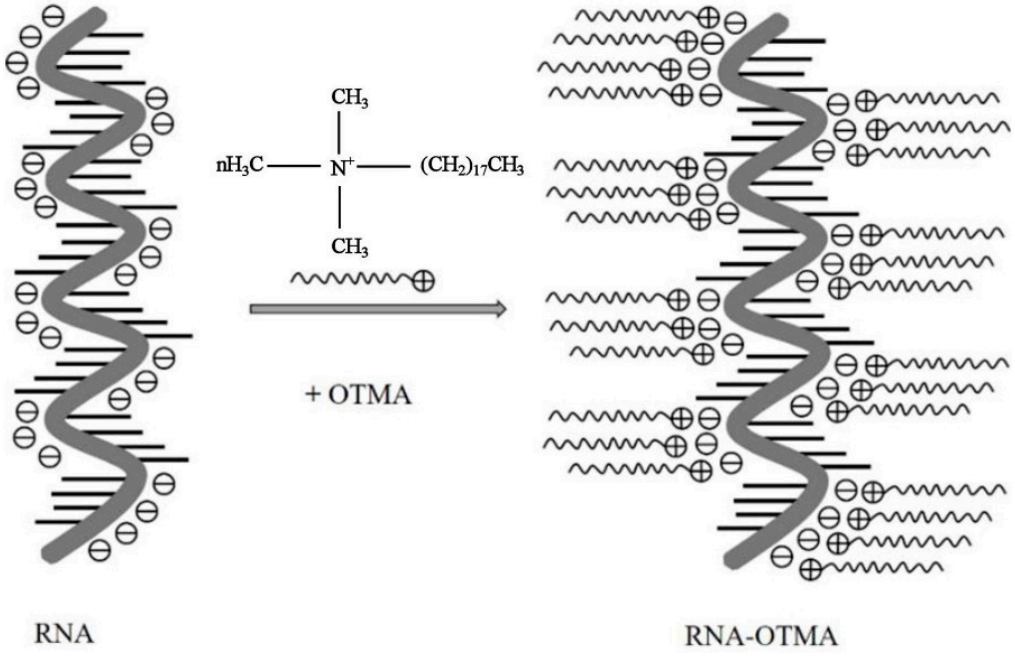

Figure 2. Schematic diagram of the preparation of RNA–OTMA lipid complexes.

2.4. Preparation of RNA–OTMA/Eu $(TTA)_3$ $(H_2O)_2$ Films and PMMA/Eu $(TTA)_3$ $(H_2O)_2$ Films

The RNA–OTMA/Eu $(TTA)_3$ $(H_2O)_2$ solution was prepared by adding 3 mL of the n-butanol solution containing Eu $(TTA)_3$ $(H_2O)_2$ to the n-butanol solution containing RNA–OTMA. The RNA–OTMA/Eu $(TTA)_3$ $(H_2O)_2$ mixture solution was prepared by spin coating method (260 rpm, 40 s) on a quartz substrate. Finally, it was dried in a vacuum drying oven at a temperature of 50 °C for 12 h. The weight percentage of Eu $(TTA)_3$ $(H_2O)_2$ in the RNA–OTMA films ranged between 8 and 35 wt.%. The preparation process of PMMA/Eu $(TTA)_3$ $(H_2O)_2$ films is the same as that of RNA–OTMA/Eu $(TTA)_3$ $(H_2O)_2$ films. It is worth mentioning that during the experiments, we increased the film thickness by slightly increasing the spin coating time at the same ratio. It turned out that the film

thickness had no significant effect on the changes in absorbance and emission intensity. Therefore, we did not carry out a special study on the thickness of the film.

2.5. Apparatus

The device for infrared-visible absorption spectra of the samples was measured by a Thermo SCIENTIFIC Fourier transform infrared spectrometer (FTIR). The UV-visible absorption spectra of the samples were tested using a SHIMADZU UV-2700 UV-Vis spectrophotometer (UV). The circular dichroism (CD) spectra of RNA complexes were measured by a Chirascan plus circular dichroism spectrometer, the reproducibility of the CD signal of thin film samples was examined by sample rotation during the test. Fluorescence emission spectra were measured using a fluorescence spectrometer at the excitation wavelength of 339 nm. In addition, the fluorescence quantum yields and fluorescence lifetimes of the samples were conducted using Edinburgh-steady state/transient fluorescence spectrometer (FS1000, UK), the quantum yield of the complex solution was determined using a 150 mm inner diameter integrating sphere mounted on the spectrometer described above. The nanosecond flash was used as an excitation light source at a wavelength of 339 nm, where the fluorescence emitted by the complex was converted to monochromatic fluorescence by a monochromator, and then shone onto a photomultiplier tube, which was then amplified by an amplifier and transmitted to the recorder.

3. Results and Discussion

3.1. Study of the Luminescence Properties of Eu (TTA)$_3$ (H_2O)$_2$ Complexes

The IR spectrum of Eu (TTA)$_3$ (H_2O)$_2$ complex solid powders was measured to analyze the bonding state in the molecules of rare earth europium complexes, as shown in Figure 3. The figure shows that the absorption peaks were found at 3650 and 3350 cm^{-1}. The broad bands were attributed to the stretching vibration of the hydroxyl group. The peaks at 1605 and 1552 cm^{-1} indicate that after the carbonyl group in the tta ligand is coordinated with Eu^{3+}, the C–O–Eu and C=O–Eu bond resonance structures successfully replaced the original C=O structure [24]. Strong absorption peaks 1605 and 1552 cm^{-1} conceal the stretching vibrational band of the C=C double bond of the trifluoromethyl group, which prevents it from being seen. The C–H bond vibration is responsible for the absorption peaks at 1417, 1304, 1255 and 1198 cm^{-1}, whereas the C–F stretching vibration is responsible for the peaks at 582 and 723 cm^{-1}.

The UV absorption spectra of Eu (TTA)$_3$ (H_2O)$_2$ complexes in butanol solution were examined to examine the molecular structure of these complexes. The n-π* and π-π* electron transitions of the ligand TTA are responsible for the Eu (TTA)$_3$ (H_2O)$_2$ complexes' absorption peaks at 260 and 339 nm, which are seen in Figure 3b. The fluorescence emission spectra of eight sets of solutions containing varying concentrations of the Eu (III) complex were examined to determine how the luminescence intensity of the films change with concentration. As seen in Figure 3c, for the $^5D_0 \rightarrow {}^7F_0$, $^5D_0 \rightarrow {}^7F_1$, $^5D_0 \rightarrow {}^7F_2$, and $^5D_0 \rightarrow {}^7F_3$ electron transitions, respectively, the emission peaks of Eu (TTA)$_3$ (H_2O)$_2$ complexes were positioned at 580, 593, 614 and 653 nm. The strongest of these causes the Eu (TTA)$_3$ (H_2O)$_2$ complex to produce red light is the transition from $^5D_0 \rightarrow {}^7F_2$ [22]. When the concentration of rare earth europium complexes increases, the luminescence intensity of Eu (TTA)$_3$ (H_2O)$_2$ complexes increases initially and then decreases. At a concentration of 10 mmol/L, the Eu (III) complex produces the brightest light, as shown in Figure 3d.

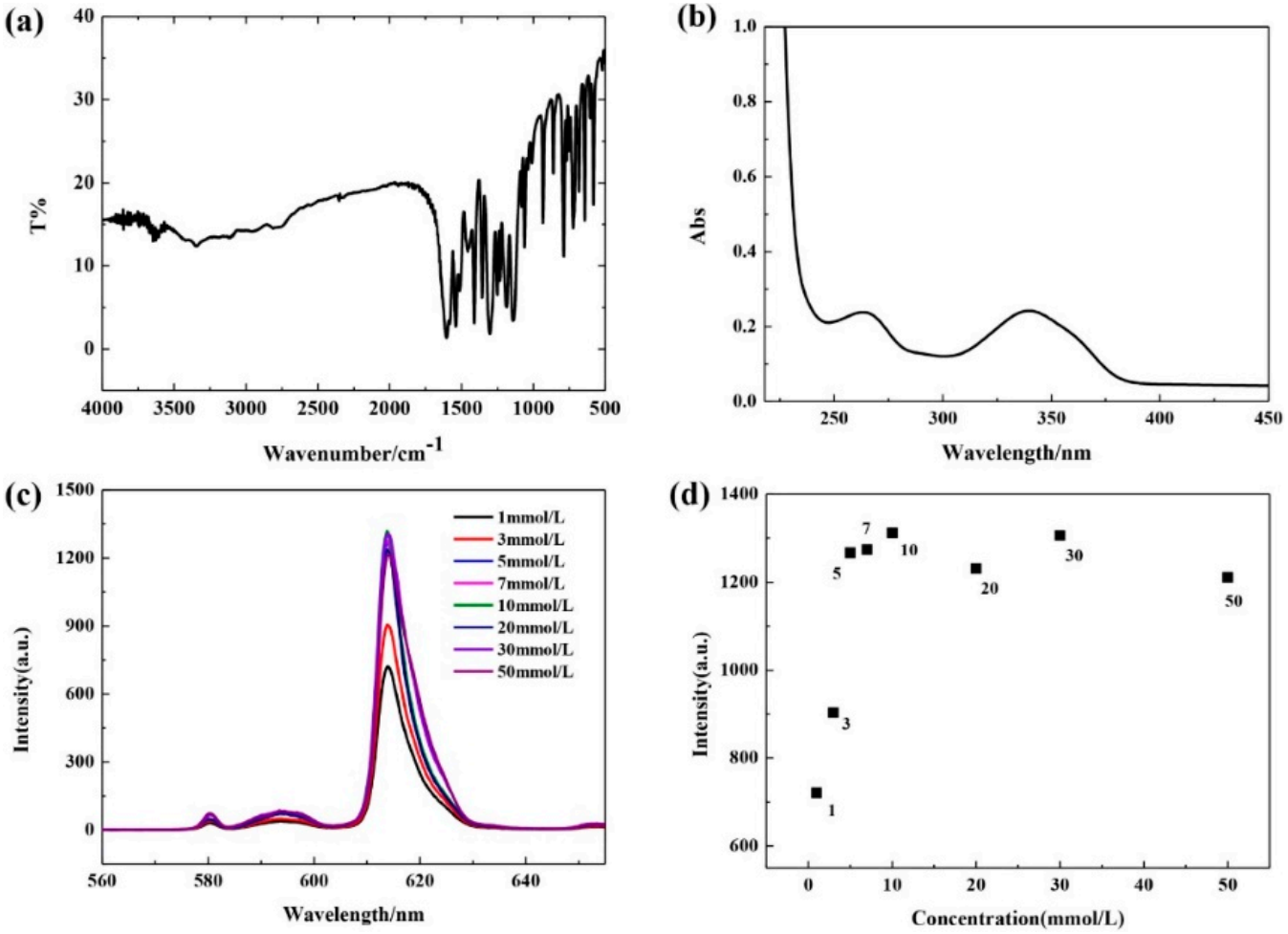

Figure 3. (**a**) Fourier transform infrared (FTIR) spectra, (**b**) UV absorption spectrum of Eu $(TTA)_3$ $(H_2O)_2$ complexes, (**c**) fluorescence emission spectrum of Eu $(TTA)_3$ $(H_2O)_2$ complex films with different concentrations under 339 excitation and (**d**) dot plot of luminescence intensity at 614 nm.

3.2. Physicochemical Properties of RNA–OTMA Lipid Composite Films

To characterize the bonding state of the RNA–OTMA lipid complex, the IR spectra of RNA and the RNA–OTMA lipid complex were tested separately. As shown in Figure 4a, RNA–OTMA has absorption peaks at 2850 and 2920 cm^{-1} compared to RNA, which is attributed to the stretching vibrations generated by the C-H of CH_2 and CH_3 groups, indicating that the OTMA group has been successfully attached to the RNA chain through the ion exchange reaction, resulting in the formation of the RNA–OTMA complex. The distinctive single-helical structure of RNA was also retained following the ion exchange procedure, as seen by the absorption peak at near 992 cm^{-1}.

The UV absorption spectra of RNA and RNA–OTMA lipid complexes were examined to determine the molecular structures of the two complexes. Both samples generated a large absorption peak at 260 nm, as seen in Figure 4b, which is due to the stacking of π-π* atoms in the purine and pyrimidine rings of the RNA structure [12]. Since the RNA–OTMA film displays exceptional optical transparency in the visible range and has no detectable absorption beyond 300 nm, it may be used in transparent electronic devices.

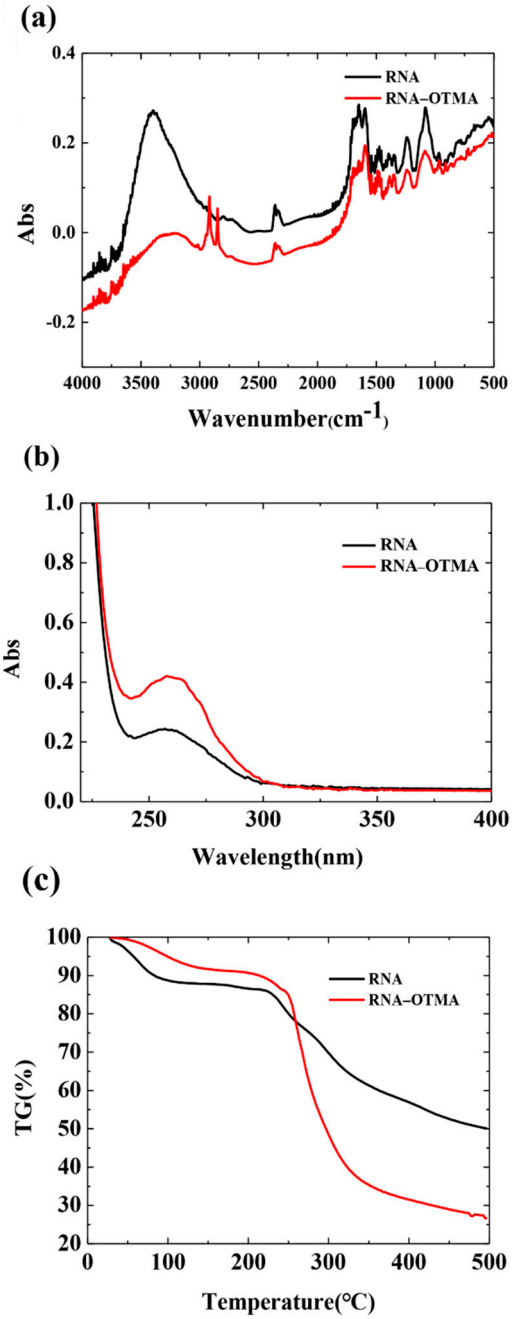

Figure 4. (**a**) Fourier transform infrared (FTIR) spectra, (**b**) UV absorption spectra in butanol solution and (**c**) TG curves of RNA and RNA–OTMA.

To investigate the thermal stability of RNA and RNA–OTMA lipid complexes, thermogravimetric analysis (TG) was conducted in a nitrogen environment. As seen in Figure 4c, when the temperature is within the range of 100 to 210 °C, the TG curve varies very minimally. The TG curve exhibits a rapid decline at 210 °C, which is the threshold at which the RNA begins to thermally breakdown. The material practically turns to carbon once the temperature reaches 400 °C; at this point, the mass loss rate is 35%. However, the temperature at which RNA–OTMA lipid compounds began to thermally decompose rose to 247 °C. It is evident from comparing the TG curves of the two that RNA's ion-exchange process increases its stability.

3.3. The Interaction between Eu $(TTA)_3$ $(H_2O)_2$ Complexes and RNA–OTMA

To investigate the interaction between the Eu (III) complex and RNA–OTMA, a mixture of RNA–OTMA and Eu $(TTA)_3$ $(H_2O)_2$ with concentration ratios of 0:1, 6:1 and 26:1, respectively, were prepared to test the UV absorption spectra of the solutions in turn, as shown in Figure 5. As can be seen from the figure, absorption bands are observed at 260 nm and 339 nm. The absorption peak at 260 nm is attributed to the absorption of bases in the RNA and the superposition of n-π^* electron transitions in the tta ligand. The π-π^* electron transitions in the tta ligand are responsible for the absorption band at about 340 nm. When the RNA–OTMA to Eu $(TTA)_3$ $(H_2O)_2$ ratio is 0:1, the Eu $(TTA)_3$ $(H_2O)_2$ complex achieves the maximum absorption at 339 nm. The absorption maximum of the Eu (III) complex exhibited a red shift of approximately 16 nm as the concentration of RNA–OTMA lipid complex rose, resulting in an absorption maximum at around 350 nm at a 26:1 ratio of RNA–OTMA to Eu $(TTA)_3$ $(H_2O)_2$. In addition, the absorbance of Eu $(TTA)_3$ $(H_2O)_2$ decreased significantly as the concentration of the RNA–OTMA lipid complex increased. By characterizing the UV absorption spectra, it can be tentatively concluded that the Eu (III) complex may have undergone some changes in the process of binding to RNA–OTMA at the bases of the RNA single strand.

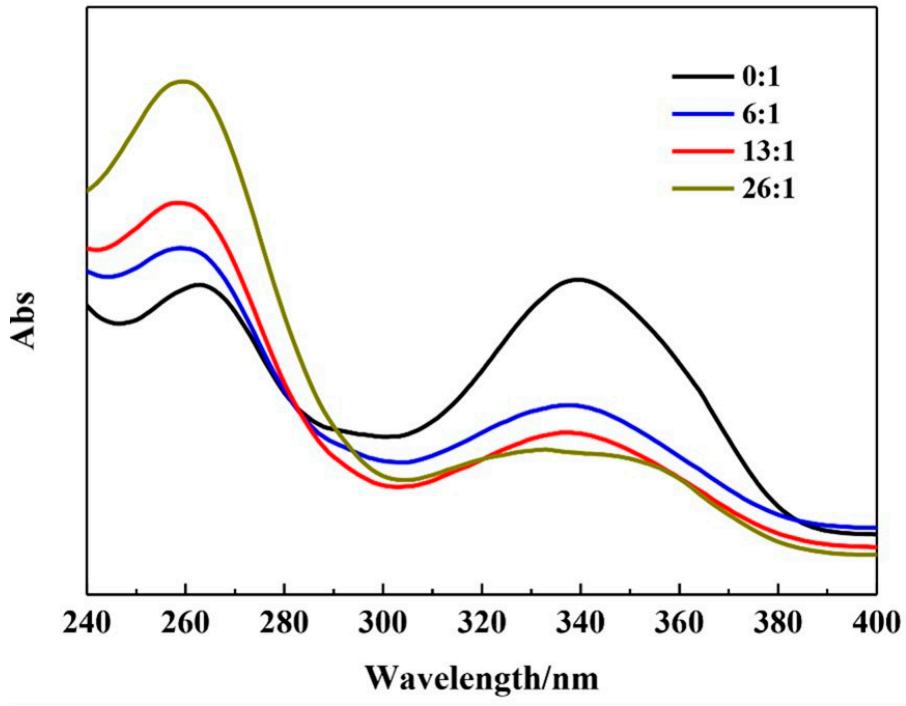

Figure 5. UV absorption spectra of different concentrations of RNA–OTMA mixed with Eu $(TTA)_3$ $(H_2O)_2$ Eu $(TTA)_3$ $(H_2O)_2$: RNA–OTMA = 0:1, 6:1, 13:1 and 26:1complexes dissolved in butanol solution.

We conducted CD spectra of RNA–OTMA and RNA–OTMA/Eu $(TTA)_3$ $(H_2O)_2$ in the solution state, which is one of the crucial methods for understanding the secondary structure of biopolymers [25], to give a thorough analysis of the interaction between the two. Figure 6 displays the CD spectra, absorption spectra and the corresponding difference spectra of the RNA–OTMA solution and the RNA–OTMA/Eu $(TTA)_3$ $(H_2O)_2$ solution, respectively. ([RNA–OTMA]: [Eu $(TTA)_3$ $(H_2O)_2$] = 4:1). As shown in Figure 6a. two negative signal peaks for RNA–OTMA were found at 235 nm and 250 nm, and one positive peak was found at 280 nm. These results are comparable with the CD spectral characteristics of the RNA complex in other studies [12]. Following that, after doping RNA–OTMA with the Eu (III) complex, certain changes in the CD spectrum of the RNA–OTMA/Eu $(TTA)_3$ $(H_2O)_2$ solution were observed. In comparison to RNA–OTMA, the two negative and one positive signal peaks at around 235, 250 and 280 nm displayed a drop in amplitude and a

notable downward shift in the position of the signal peaks. Furthermore, in the CD and difference spectra of RNA–OTMA/Eu $(TTA)_3$ $(H_2O)_2$, it can be observed that the absorption peaks appearing around 340 nm correspond to each other with the tta ligand absorption band around 340 nm in Figure 6b, which indicates that the π-π* electron transition of the tta ligand is influenced by the RNA–OTMA lipid complex, thus verifying that an interaction between the RNA–OTMA single chain and the Eu $(TTA)_3$ $(H_2O)_2$, complex occurs, i.e., the Eu (III) complex is embedded or semi-embedded in the groove between the bases in the RNA–OTMA molecule, hindering the molecular transition.

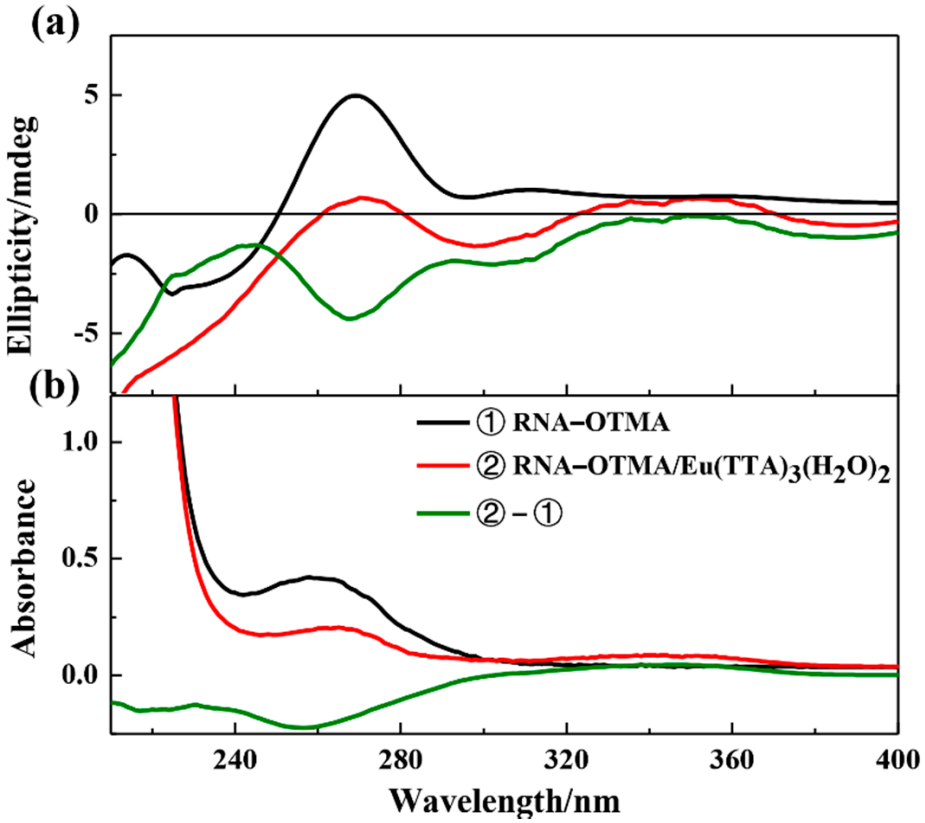

Figure 6. (**a**) CD spectra and (**b**) absorption spectra, and difference spectra of RNA–OTMA solution, RNA–OTMA/Eu $(TTA)_3$ $(H_2O)_2$ solution. ([RNA–OTMA]: [Eu $(TTA)_3$ $(H_2O)_2$] = 4:1).

3.4. Emission Properties of RNA–OTMA/Eu $(TTA)_3$ $(H_2O)_2$ Films

In order to discuss the effect of different Eu $(TTA)_3$ $(H_2O)_2$ complex contents on the luminescence intensity, the emission spectra of RNA–OTMA lipid complexes doped with Eu $(TTA)_3$ $(H_2O)_2$ complexes at different ratios were tested (as shown in Figure 7a). The figure shows that emission peaks are observed at 580, 593, 614 and 653 nm with $^5D_0 \rightarrow {}^7F_0$, $^5D_0 \rightarrow {}^7F_1$, $^5D_0 \rightarrow {}^7F_2$ and $^5D_0 \rightarrow {}^7F_3$ electron transitions, respectively, among which $^5D_0 \rightarrow {}^7F_2$ has the strongest transition, making the Eu $(TTA)_3$ $(H_2O)_2$ complex emit red light. Figure 7b shows the dot plot of luminescence intensity of Eu $(TTA)_3$ $(H_2O)_2$ complex films with different concentrations at 614 nm, from which it can be seen that the luminescence intensity shows an enhancing trend with the increasing content of RNA–OTMA in RNA–OTMA/Eu $(TTA)_3$ $(H_2O)_2$, and Eu $(TTA)_3$ $(H_2O)_2$ complex had the brightest luminescence when the ratio of RNA–OTMA to Eu $(TTA)_3$ $(H_2O)_2$ reached 4:1.

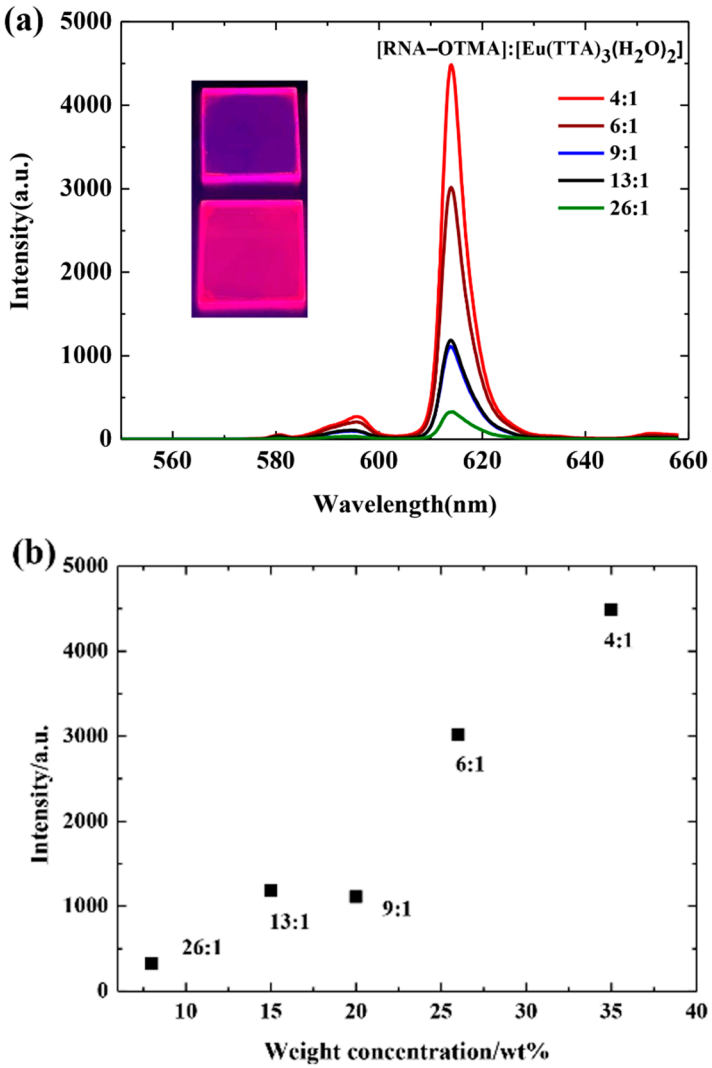

Figure 7. (**a**) Fluorescence emission spectra of different concentrations of Eu $(TTA)_3$ $(H_2O)_2$ complexes in RNA–OTMA (extended figure shows the comparison of the luminescence of [RNA–OTMA]: [Eu $(TTA)_3$ $(H_2O)_2$] = 0:1 film (top) and [RNA–OTMA]: [Eu $(TTA)_3$ $(H_2O)_2$] = 4:1 film (bottom) under UV lamp). (**b**) Dot plot of luminescence.

By contrasting the RNA–OTMA lipid complexes with PMMA complex films, the impact of RNA–OTMA on the luminescence characteristics of Eu $(TTA)_3$ $(H_2O)_2$ complex was further confirmed. The fluorescence emission spectrum of the films and the UV spectrum of the solution of RNA–OTMA/Eu $(TTA)_3$ $(H_2O)_2$ and PMMA/Eu $(TTA)_3$ $(H_2O)_2$ complex were measured. The concentration ratios of RNA–OTMA and PMMA to Eu (III) were both 4:1. According to Figure 8a, both films exhibit absorption peaks at 339 nm, which are attributable to the electron π-π^* transition in the ligand TTA. The absorbance of the ligand at this excitation wavelength is also close because both films contain an identical number of Eu $(TTA)_3$ $(H_2O)_2$ complexes. Interestingly, the fluorescence intensity of the Eu $(TTA)_3$ $(H_2O)_2$ combination in the RNA–OTMA films was much higher than that of the PMMA films, as shown in Figure 8b. This demonstrates that, when compared to the commonly used polymer PMMA, the biomaterial RNA–OTMA lipid combination can significantly increase the luminescence intensity of Eu $(TTA)_3$ $(H_2O)_2$ complexes.

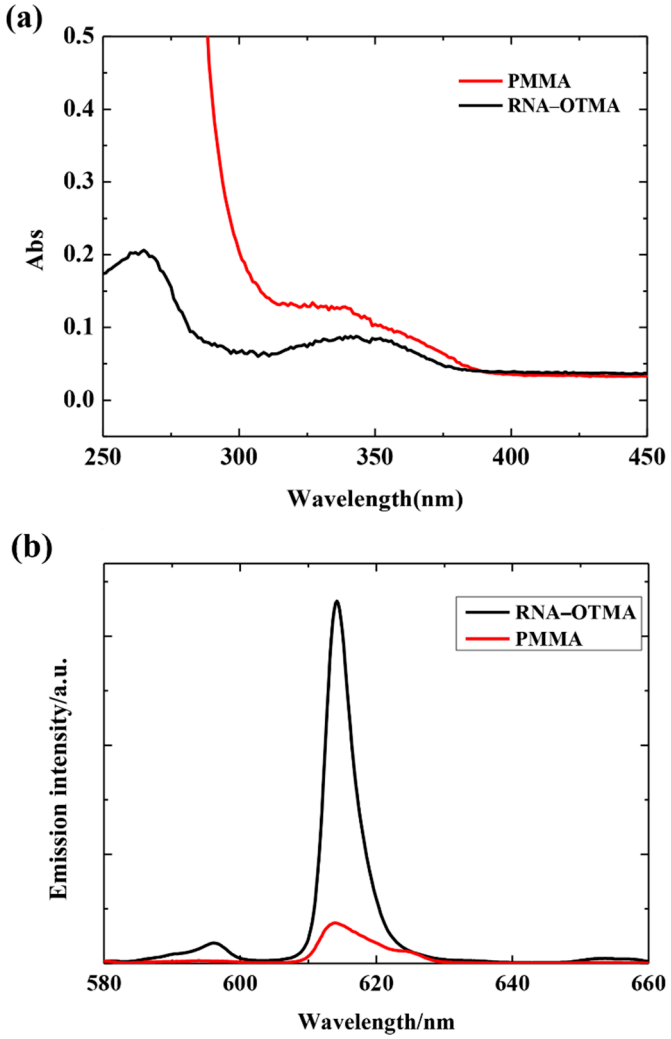

Figure 8. (**a**) UV absorption spectra of PMMA/Eu $(TTA)_3$ $(H_2O)_2$ and RNA–OTMA/Eu $(TTA)_3$ $(H_2O)_2$ in butanol solution and (**b**) fluorescence emission spectra of the films.

In order to conduct a thorough investigation, we measured the RNA–OTMA/PMMA films' fluorescence emission spectra when Eu $(TTA)_3$ $(H_2O)_2$ was added at various ratios. Figure 9a shows the fluorescence intensity at various [RNA–OTMA]: [Eu $(TTA)_3$ $(H_2O)_2$] ratios of 13:1, 9:1, 6:1 and 4:1. As a reference, the fluorescence intensity of PMMA/Eu $(TTA)_3$ $(H_2O)_2$ films at the same ratio was also measured, as shown in Figure 9b. According to Figure 9a, the luminescence intensity of RNA–OTMA lipid complex films increased progressively with an increase in RNA–OTMA content before reaching its maximum when the ratio of RNA–OTMA to Eu $(TTA)_3$ $(H_2O)_2$ was 4:1; According to Figure 9b, the luminescence intensity of PMMA/Eu $(TTA)_3$ $(H_2O)_2$ films achieves its optimum when the ratio of PMMA to Eu $(TTA)_3$ $(H_2O)_2$ was 13:1. However, the luminescence intensity is much lower than that of RNA–OTMA-doped rare-earth europium complexes. This suggests that, when compared to the conventional polymer PMMA, RNA–OTMA can significantly suppress the concentration quenching of the Eu (III) complex emission. This is because the base structure of RNA has several grooves of various diameters, and the existence of these grooves creates a large surface area for Eu $(TTA)_3$ $(H_2O)_2$ complex at the nanoscale [26,27]. In the thin film state, Eu $(TTA)_3$ $(H_2O)_2$ complexes can form complexes with RNA–OTMA by embedding or semi-embedding in the base-to-base grooves of the RNA–OTMA helical structure, suppressing the non-radiative deactivation caused by molecular vibrations, resulting in increased fluorescence intensity of Eu^{3+} [26]. Meanwhile, the Eu $(TTA)_3$ $(H_2O)_2$ complexes embedded in the base-to-base groove on the RNA–OTMA chain would separate

Eu^{3+} ions from each other, making it more difficult for them to aggregate, which would increase the luminescence intensity.

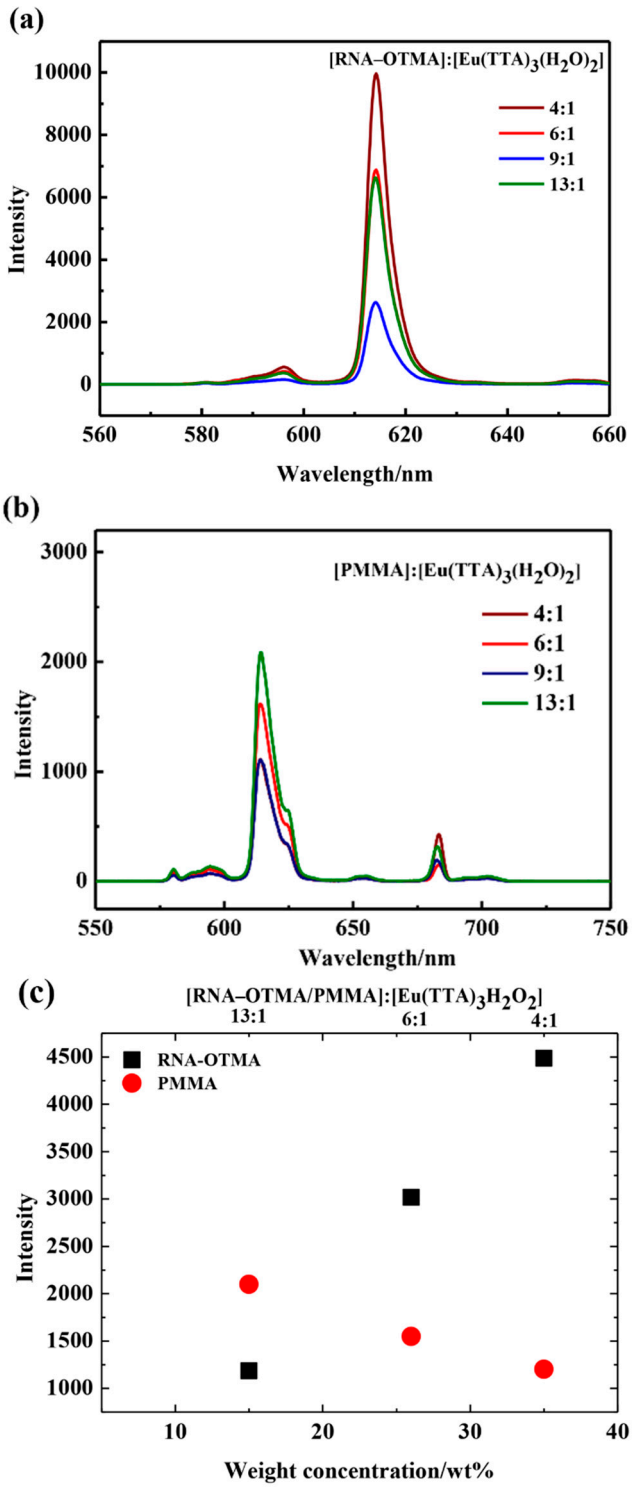

Figure 9. Fluorescence emission spectra of different concentrations of Eu $(TTA)_3$ $(H_2O)_2$ complexes in (**a**) RNA–OTMA and (**b**) PMMA, and (**c**) dot plots of fluorescence emission intensity of RNA–OTMA/Eu films and PMMA/Eu films at different concentration ratios. (The weight percentages of Eu $(TTA)_3$ $(H_2O)_2$ complexes ranged from 15% to 35%, and the excitation wavelength was 339 nm).

The fluorescence emission lifetimes and quantum yields of the films were measured to evaluate their photophysical characteristics. First, the effect of RNA–OTMA lipid complex doped with Eu $(TTA)_3$ $(H_2O)_2$ complex on the fluorescence emission lifetime was initially investigated, and the fluorescence emission lifetime of the films was measured at a 4:1 ratio of RNA–OTMA/PMMA to Eu $(TTA)_3$ $(H_2O)_2$, as shown in Figure 10a. The picture shows that the decay of the emission intensity of RNA–OTMA lipid complex films is substantially slower than that of PMMA complex films at the same Eu (III) complex concentration, which may be a sign that RNA–OTMA complex films have a longer fluorescence lifespan than PMMA complex films. The luminescence lifetime can be fitted by the following double exponential function:

$$I_t = A + B_1 exp(-t/\tau_1) + B_2 exp(-t/\tau_2) \quad (1)$$

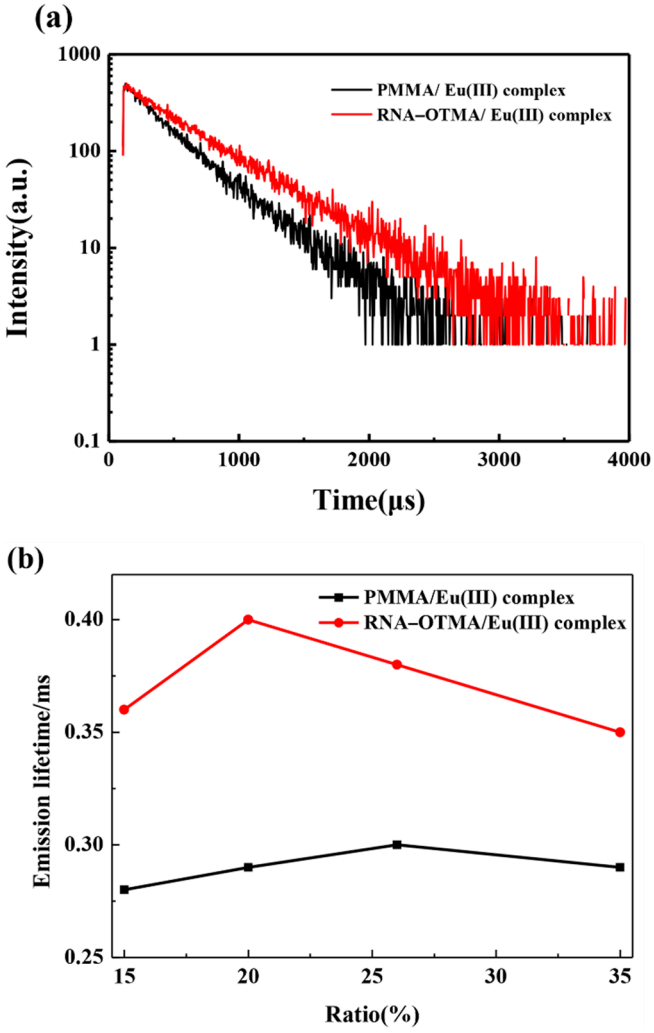

Figure 10. (**a**) Fluorescence lifetime of the films at [RNA–OTMA/PMMA]: [Eu $(TTA)_3$ $(H_2O)_2$] = 4:1 (**b**) Fluorescence lifetimes of RNA–OTMA/Eu complex films and PMMA/Eu complex films at different Eu (III) complex contents.

A in Equation (1) is the luminous intensity at time 0, 1 and 2 are the short decay and long decay components, respectively, and the coefficients B_1 and B_2 are fitting constants. In order to investigate the effect of fluorescence emission lifetime of RNA–OTMA lipid complexes doped with Eu (III) complexes in depth, the fluorescence emission lifetimes of RNA–OTMA complexes and PMMA complex films with different Eu (III) complex contents were tested separately, as shown in Figure 10b. It can be seen from the figure that under the excitation of 339 nm wavelength, the optical lifetimes of the PMMA doped Eu (III) complex films were approximately 300 μs, while the fluorescence lifetimes of the RNA–OTMA-

doped Eu (III) complex films were much longer, increasing to 400 μs, which were about 100 μs higher than that of the PMMA complex films. Because of the unique single-helix structure of RNA, when Eu (III) complexes are combined with RNA–OTMA, the Eu (III) complexes obtain entrenched in the RNA–OTMA matrix, inhibiting the vibrational and aggregation quenching of the Eu (III) ions formed in the excited state. Meanwhile, it was observed that the complex films of RNA–OTMA-doped Eu (III) complex maintained high luminescence intensity at the Eu (III) complex content up to 35 wt.%, which also indicated that the RNA–OTMA matrix prevented the aggregation of Eu (III) complex and similarly enhanced the luminescence performance of the complex films. Furthermore, previous research has shown that highly symmetric Eu (III) complexes have lower radiation rate constants, and thus, longer emission lifetimes [28]. Based on the findings, we can speculate that interaction with RNA–OTMA causes the structure of the Eu (III) complex to become more symmetrical, thereby extending the fluorescence emission lifespan of RNA–OTMA complex films.

To better understand the properties of the films, the fluorescence quantum yields of RNA–OTMA/Eu $(TTA)_3$ $(H_2O)_2$ films and PMMA/Eu $(TTA)_3$ $(H_2O)_2$ films at various ratios were measured, as shown in Figure 11. At low concentrations of Eu (III) complex content, the fluorescence quantum yield was around 15% ([RNA–OTMA]: [Eu $(TTA)_3$ $(H_2O)_2$] = 26:1). When the ratio of RNA–OTMA to Eu (III) complexes was 4:1, the fluorescence quantum yield approached 60% and the quantum yield of the films increased with the rise in Eu $(TTA)_3$ $(H_2O)_2$ concentration. This is because the RNA–OTMA lipid complex prevented the Eu $(TTA)_3$ $(H_2O)_2$ complex burst, which increased the fluorescence quantum yield, by preventing the aggregation of Eu^{3+} ions. In comparison to the common polymer PMMA, the experimental results demonstrate that the RNA–OTMA lipid combination may significantly increase the quantum yield of the Eu $(TTA)_3$ $(H_2O)_2$ complex. As the ratio of RNA–OTMA to Eu (III) complex changes, the structure of the Eu $(TTA)_3$ $(H_2O)_2$ complex likewise becomes more symmetrical.

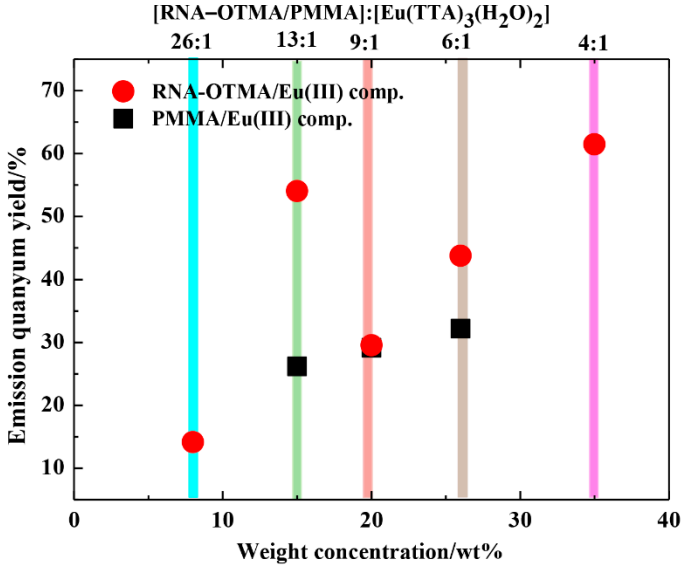

Figure 11. Fluorescence quantum yields of RNA–OTMA/Eu $(TTA)_3$ $(H_2O)_2$ films and PMMA/Eu $(TTA)_3$ $(H_2O)_2$ films.

4. Conclusions

In the present work, a novel RNA-based luminescent composite was prepared by doping RNA–OTMA lipid complexes with different concentrations of Eu $(TTA)_3$ $(H_2O)_2$ complexes. First, the interaction between RNA–OTMA and Eu $(TTA)_3$ $(H_2O)_2$ complexes was investigated, and the Eu (III) complexes were initially inferred to be possibly embedded or semi-embedded in RNA–OTMA by characterization of UV absorption spectra. Then,

the previous inference was further verified by the characterization of the CD spectra of the complex solution. Next, the effect of RNA–OTMA lipid complexes on the luminescence properties of Eu $(TTA)_3$ $(H_2O)_2$ complexes was investigated, and the complex films were prepared by adding conventional polymer PMMA for comparison. The experimental results showed that the RNA–OTMA lipid complexes could significantly enhance the luminescence intensity of Eu $(TTA)_3$ $(H_2O)_2$ complexes in the thin film state. When the RNA–OTMA to Eu $(TTA)_3$ $(H_2O)_2$ ratio was 4:1, the fluorescence intensity of the RNA–OTMA lipid complex film was highest. In contrast to the polymer material PMMA, the luminescence intensity of Eu $(TTA)_3$ $(H_2O)_2$ complexes in RNA–OTMA lipid complex films was much higher than that of PMMA films at the same concentration ratios. In addition, the fluorescence lifetimes and fluorescence quantum yield of RNA–OTMA complex films were also significantly better than those of PMMA complex films. It further indicates that RNA–OTMA lipid complexes as biomaterials can improve the luminescence intensity of fluorescent materials and have the potential to be used in optoelectronic devices.

Author Contributions: N.Z. and R.C. designed and carried out the experiment. N.Z., R.C. and S.W. processed the test data. With the help of L.L., N.Z., S.L., Z.Y., L.L., Z.Y. and Q.L. wrote and completed the paper. J.W., Z.L. and T.J. supervised this project. All authors have read and agreed to the published version of the manuscript.

Funding: This research is supported by Beijing Natural Science Foundation (No. 2202018), General Project of Beijing Municipal Education Commission Science and Technology Program (No. KM202010015004), the Key Area Research and Development Program of Guangdong Province (Grant no. 2020B0101020002) and the GBA National Institute for Nanotechnology Innovation (Grant no. 2020GN0106), Research and development of intelligent packaging for cultural relics (Ed202001), Construction and application trans-formation of cross media cloud platform for printing and packaging anti-counterfeiting and traceability (27170121005), National Natural Science Foundation of China (No. 21604005), the general project of fundamental research of BIGC (No. Eb202001, 20190122041, 22150122042, 22150122034), Initial funding for the Doctoral Program of BIGC (No. 27170121001/002), and the general project of science and technology of Beijing Municipal Education Commission (No. KM202110015008).

Institutional Review Board Statement: Not applicable.

Informed Consent Statement: Not applicable.

Data Availability Statement: Not applicable.

Conflicts of Interest: The authors declare no conflict of interest.

References

1. Kesama, M.R.; Dugasani, S.R.; Gnapareddy, B.; Park, S.H. Spectroscopic and Capacitance Characteristics of DNA Thin Layers Embedded with Semiconducting ZnO and CuO Nanoparticles. *ACS Appl. Electron. Mater.* **2019**, *1*, 991–1002. [CrossRef]
2. Lin, P.-C.; Wong, Y.-T.; Su, Y.-A.; Chen, W.-C.; Chueh, C.-C. Interlayer Modification Using Eco-friendly Glucose-Based Natural Polymers in Polymer Solar Cells. *ACS Sustain. Chem. Eng.* **2018**, *6*, 14621–14630. [CrossRef]
3. Fukuzaki, A.; Kawai, H.; Sano, T.; Takehara, K.; Nagamura, T. Efficient Upconversion by Highly Water-Soluble Cationic Sensitizer and Emitter in Aqueous Solutions with DNA. *ACS Biomater. Sci. Eng.* **2017**, *3*, 1809–1814. [CrossRef]
4. Jin, L.; Tan, Y.-L.; Wu, Y.; Wang, X.; Shi, Y.-Z.; Tan, Z.-J. Structure folding of RNA kissing complexes in salt solutions: Predicting 3D structure, stability, and folding pathway. *RNA* **2019**, *25*, 1532–1548. [CrossRef]
5. Zhao, X.; Wu, H.; Guo, B.; Dong, R.; Qiu, Y.; Ma, P.X. Antibacterial anti-oxidant electroactive injectable hydrogel as self-healing wound dressing with hemostasis and adhesiveness for cutaneous wound healing. *Biomaterials* **2017**, *122*, 34–47. [CrossRef]
6. Cui, L.; Wu, J.; Ju, H. Electrochemical sensing of heavy metal ions with inorganic, organic and bio-materials. *Biosens. Bioelectron.* **2015**, *63*, 276–286. [CrossRef] [PubMed]
7. Zou, J.; Li, S.; Wang, H.; Wang, W.; Shi, Z.; Jiang, Y.; Cui, Z.; Yan, D. High-k polymer materials containing cyclic carbonate as gate dielectrics for application in low-voltage operating organic thin-film transistors. *J. Mater. Chem. C* **2019**, *7*, 15357–15363. [CrossRef]
8. Kaplan, D.L. Introduction to biopolymers from renewable resources. In *Biopolymers from Renewable Resources*; Springer: Berlin/Heidelberg, Germany, 1998; pp. 1–29.
9. Mohanty, A.K.; Misra, M.; Drzal, L.T. *Natural Fibers, Biopolymers, and Biocomposites*; CRC Press: Boca Raton, FL, USA, 2005.

10. Klemm, D.; Heublein, B.; Fink, H.-P.; Bohn, A. Cellulose: Fascinating Biopolymer and Sustainable Raw Material. *Angew. Chem. Int. Ed.* **2005**, *44*, 3358–3393. [CrossRef]
11. Hagen, J.A.; Li, W.; Steckl, A.J.; Grote, J.G. Enhanced emission efficiency in organic light-emitting diodes using deoxyribonucleic acid complex as an electron blocking layer. *Appl. Phys. Lett.* **2006**, *88*, 171109. [CrossRef]
12. Liang, L.; Fu, Y.; Li, L.; Zheng, H.; Wei, X.; Wei, Y.; Kobayashi, N. RNA–CTMA Dielectrics in Organic Field Effect Transistor Memory. *Appl. Sci.* **2018**, *8*, 887. [CrossRef]
13. Eliseeva, S.V.; Bünzli, J.-C.G. Lanthanide luminescence for functional materials and bio-sciences. *Chem. Soc. Rev.* **2009**, *39*, 189–227. [CrossRef] [PubMed]
14. Bünzli, J.-C.G. Lanthanide light for biology and medical diagnosis. *J. Lumin.* **2016**, *170*, 866–878. [CrossRef]
15. De Bettencourt-Dias, A. Lanthanide-based emitting materials in light-emitting diodes. *Dalton Trans.* **2007**, *22*, 2229–2241. [CrossRef] [PubMed]
16. Kido, J.; Hayase, H.; Hongawa, K.; Nagai, K.; Okuyama, K. Bright red light-emitting organic electroluminescent devices having a europium complex as an emitter. *Appl. Phys. Lett.* **1994**, *65*, 2124–2126. [CrossRef]
17. Ogasawara, K.; Nakamura, K.; Kobayashi, N. Thermally controlled dual-mode display media with red-green-blue coloration and fluorescence via energy transfer between emission materials and leuco dyes. *J. Mater. Chem. C* **2016**, *4*, 4805–4813. [CrossRef]
18. Butler, S.J.; Parker, D. Anion binding in water at lanthanide centres: From structure and selectivity to signalling and sensing. *Chem. Soc. Rev.* **2013**, *42*, 1652–1666. [CrossRef]
19. Miyata, K.; Konno, Y.; Nakanishi, T.; Kobayashi, A.; Kato, M.; Fushimi, K.; Hasegawa, Y. Chameleon Luminophore for Sensing Temperatures: Control of Metal-to-Metal and Energy Back Transfer in Lanthanide Coordination Polymers. *Angew. Chem. Int. Ed.* **2013**, *52*, 6413–6416. [CrossRef]
20. Ogata, S.; Shimizu, T.; Ishibashi, T.; Ishiyone, Y.; Hanami, M.; Ito, M.; Ishii, A.; Kawaguchi, S.; Sugimoto, K.; Hasegawa, M. Water-soluble lanthanide complexes with a helical ligand modified for strong luminescence in a wide pH region. *New J. Chem.* **2017**, *41*, 6385–6394. [CrossRef]
21. Kobayashi, N.; Uemura, S.; Kusabuka, K.; Nakahira, T.; Takahashi, H. An organic red-emitting diode with a water-soluble DNA–polyaniline complex containing $Ru(bpy)_3^{2+}$. *J. Mater. Chem.* **2001**, *11*, 1766–1768. [CrossRef]
22. Nakamura, K.; Minami, H.; Sagara, A.; Itamoto, N.; Kobayashi, N. Enhanced red emissions of europium(iii) chelates in DNA–CTMA complexes. *J. Mater. Chem. C* **2018**, *6*, 4516–4522. [CrossRef]
23. Minami, H.; Itamoto, N.; Watanabe, W.; Li, Z.; Nakamura, K.; Kobayashi, N. Chiroptical property enhancement of chiral Eu(III) complex upon association with DNA-CTMA. *Sci. Rep.* **2020**, *10*, 18917. [CrossRef]
24. Peng, D. *Synthesis Characterization and LED of a List of -Diketonate-Europiem(III) Complex*; Hunan University: Changsha, China, 2013.
25. Steckl, A.J.; Spaeth, H.; You, H.; Gomez, E.; Grote, J. DNA as an optical material. *Opt. Photonics News* **2011**, *22*, 34–39. [CrossRef]
26. Miljanic', S.; Kenđel, A.; Novak, M.; Deliqeorqiev, T.G.; Crnolatac, I.; Piantanida, I.; Chiş, V. Distinguishing binding modes of a new phosphonium dye with DNA by surface-enhanced Raman spectroscopy. *RSC Adv.* **2016**, *6*, 41927–41936. [CrossRef]
27. Kawabe, Y.; Wang, L.; Nakamura, T.; Ogata, N. Thin-film lasers based on dye-deoxyribonucleic acid-lipid complexes. *Appl. Phys. Lett.* **2002**, *81*, 1372–1374. [CrossRef]
28. Nakamura, K.; Hasegawa, Y.; Kawai, H.; Yasuda, N.; Kanehisa, N.; Kai, Y.; Nagamura, T.; Yanagida, A.S.; Wada, Y. Enhanced Lasing Properties of Dissymmetric Eu(III) Complex with Bidentate Phosphine Ligands. *J. Phys. Chem. A* **2007**, *111*, 3029–3037. [CrossRef]